Modeling of Reaction-Induced Flow Maldistributions in Packed Beds

Friedemann Stroh and Vemuri Balakotaiah
Dept. of Chemical Engineering, University of Houston, Houston, TX 77204

This work examines reaction-induced flow maldistributions in adiabatic, downflow packed beds. Using linear stability analysis it is shown that for the case of a constant heat source, the uniform flow loses stability when a certain dimensionless group, the Darcy buoyancy number, exceeds a critical value. Center manifold theory is used to analyze the local bifurcation picture for the case of a simple and double zero eigenvalue. It is found that for large Peclet numbers, all the bifurcations from the uniform solution are subcritical in nature and are unstable locally. Orthogonal collocation and continuation techniques are combined with the local theory to determine the various branches of bifurcating solutions. The temperature and flow distributions of stable and unstable solution branches are presented for several aspect ratios and Peclet numbers. Numerical simulations predict direct transitions from uniform flow to periodic or chaotic flows. It is also found that there is a wide range of the Darcy buoyancy number in which the uniform and maldistributed flows are stable and coexist.

Introduction

Packed beds with down flow are used in many applications. One or more fluids flow through a reactor that is filled with a catalyst packing, react to the desired product, and leave the vessel. In designing this process, one usually assumes a one-dimensional flow. In many cases, the actual flow is one-dimensional, but often flow maldistributions are observed that lead to hot spots, if the reaction is exothermic. Jaffe (1976) describes such steady-state hot spots in commercial packed-bed reactors. These hot spots can damage the catalyst and the reactor vessel. Flow maldistributions lead also to inhomogeneities in the product because of the spread in residence times. Therefore, it is very important to understand the nature and origin of these hot spots and to estimate their size.

Jaffe (1976) explained and simulated the hot spots with limited regions of low flow in a packed bed. He estimated the velocity and the lateral extent of the low flow regions by matching data from a commercial hydrogenation process with his numerical simulations. These zones with low velocities are usually explained by inhomogeneities of the packing, but this explanation is not always satisfying. We provide here a simple model that predicts slow and fast flow regions and the associated hot and cold spots for homogeneous packed beds with down flow. The model determines for what parameter values hot spots occur as well as their size and distribution.

The flow maldistributions modeled here are driven by local heat sources due to chemical reactions. The heat liberated by the reaction increases the temperature in the direction of flow. This change in temperature causes density variations in the fluid. If the density decreases in the direction of the gravity, the buoyancy force can lead to instabilities (Rayleigh instability). This phenomenon is similar to the convective instabilities due to an applied temperature gradient which have been the subject of many previous studies (Gershuni and Zhukhovitskii, 1976).

The linear stability of a semi-infinite porous layer with large upward flow has been investigated by Wooding (1960). Sutton (1970) presented results for very small flow rates. Nield (1975) analyzed the stability of flow through a porous medium as a special case of convective instability in systems with nonuniform thermal gradients. Homsy and Sherwood (1976) examined the stability of flows in porous media with the assumption of constant velocity and constant temperature at the upper and lower boundary. Jones and Persichetti (1986) extended these results to other boundary conditions, and Nield (1987) analyzed the effect of boundary conditions on the stability of the through flow. All these authors assumed infinite length in directions perpendicular to the flow and that the temperature gradient is due to the boundary conditions. Their results give

the critical Rayleigh numbers at which the uniform flow becomes unstable. Reda (1988) analyzed a porous cylinder which is heated by a rod in the middle and determined the streamlines and isotherms experimentally and numerically using a two-dimensional model.

There have been several studies on convective instabilities that are due to local heat sources in closed systems. Gasser and Kazimi (1976) used linear stability to determine the onset of convection in a porous layer with internal heat generation. Tveitereid (1977) obtained numerically stable two- and three-dimensional convective solutions in a horizontal porous layer with internal heat sources. Reaction-driven convection in a porous cylinder or box without through flow has been analyzed by Bdzil and Frisch (1980), Steinberg and Brand (1983), Kordylewski and Krajewski (1984), Stewart and Dona (1988), Prasad (1987), and Viljoen and Hlavacek (1987). All these authors find various circulating flows similar to the convection rolls observed in the Benard problem and corresponding hot spots for the closed system.

In contrast to these, there have been relatively few studies on reaction-driven convective instabilities in open systems. Hadim and Burmeister (1988) determine the stability of uniform flow in a porous medium with down flow heated by solar energy. Because of their fixed-temperature boundary conditions at inlet and outlet, their model cannot be used to simulate packed-bed reactors. Gatica et al. (1988, 1989) analyzed a two-dimensional model of flow with reaction in a porous box for small Peclet numbers. None of these previous studies examined the local bifurcation picture or the flow patterns in the case of through flow.

In this work, we develop and analyze a simple model for simulating maldistributions of the down flow in packed beds due to an internal heat source. We use the linear stability theory to determine when the uniform flow becomes unstable for the case of a constant heat source. To find the two-dimensional solutions, we first determine the local bifurcation picture using the Center Manifold reduction. We then use the local result as a guide and obtain the global bifurcation diagrams with orthogonal collocation and continuation techniques. The flow patterns and temperature distributions corresponding to the new two dimensional solutions are presented. The results of the numerical simulations are used to construct a phase diagram which can be used to determine the parameter values for which flow maldistributions may exist.

Mathematical Model

In this section, we derive a simple model for an adiabatic packed bed with down flow. First we assume for simplicity that there is only one fluid or that the properties of several fluids can be lumped into one effective fluid. In general, a separate energy balance must be considered for the fluid and the solid in the reactor. However, Vortmeyer et al. (1974) showed that a single energy balance where the fluid and the packing is treated as a continuous medium gives reliable results, if the lumped parameters are chosen properly. This simplification is commonly used in the analysis of flow in porous media. We use this assumption for the flow with reaction as well. We further assume that the reactant consumption is negligible, i.e., the concentration remains constant (so we can neglect all concentration dependencies and ignore the species balance). The next simplification is that the reaction has a zero activation energy. This is equivalent to a constant heat source in the packed bed. For the continuity equation and the momentum balance, we use the usual assumptions that Darcy's law and the Boussinesq approximation are valid and that the porous medium Prandtl number is large. The problem is then described by the three equations:

$$\nabla \cdot \boldsymbol{u} = 0 \tag{1}$$

$$\nabla p = -\frac{\mu}{\kappa}\boldsymbol{u} + \rho_0[1 - b(T - T_0)]g\boldsymbol{e}_z \tag{2}$$

$$\rho_m C_{pm}\frac{\partial T}{\partial t} + \rho_f C_{pf}\boldsymbol{u}\cdot\nabla T = \lambda_{\text{eff}}\nabla^2 T + S \tag{3}$$

where $\boldsymbol{u}$ is the superficial velocity in the packed bed and S is the constant source term. For packed beds with uniform size particles, the permeability κ may be related to the particle diameter D_p and the void fraction ϵ by the expression (Bird et al., 1960):

$$\kappa = \frac{D_p^2\epsilon^3}{150(1-\epsilon)^2} \tag{4}$$

The boundary conditions at the adiabatic walls of the reactor are given by

$$u_s = 0 \quad \frac{\partial T}{\partial s} = 0 \quad \text{at} \quad s = 0, D \tag{5}$$

where u_s is the horizontal component of the velocity vector. For the boundary conditions in axial direction we have different possibilities. We can specify either the pressure or the velocity at the inlet and outlet. The most realistic of the four possibilities is the one with fixed inlet velocity and fixed outlet pressure. For the temperature, we use boundary conditions of Hulburt type (Hulburt, 1944), instead of the more common Danckwerts boundary conditions. As we will show later, the Hulburt boundary conditions simplify the numerical calculations, and for large Peclet numbers both boundary conditions give nearly identical results. These boundary conditions are:

$$\begin{aligned} &T = T_0 \quad u_L = u_0 \quad \text{at} \quad L = 0 \\ &p = p_1 \quad \frac{\partial T}{\partial L} = 0 \quad \text{at} \quad L = L_1 \end{aligned} \tag{6}$$

To cast the equations in dimensionless form, we define the new quantities:

$$\begin{aligned} x &= \frac{s}{L_1} & z &= \frac{L}{L_1} \\ v &= \frac{u}{u_0} & y &= \frac{\rho_0 C_{pf} u_0 (T - T_0)}{SL_1} \\ \tau &= \frac{tu_0}{L}\frac{\rho_f C_{pf}}{\rho_m C_{pm}} & Pe &= \frac{\rho_f C_{pf} u_0 L}{\lambda_{eff}} \\ \Lambda &= \frac{SL_1 g\kappa b}{\mu_0 u_0^2 C_{pf}} & \alpha &= \frac{L_1}{D} \\ \Pi &= \frac{\kappa(p - \rho_0 g z L_1)}{\mu_0 u_0 L_1} & \Pi_0 &= \frac{\kappa(p_1 - \rho_0 g L_1)}{\mu_0 u_0 L_1} \end{aligned} \tag{7}$$

The dimensionless parameters are the Darcy buoyancy number, Λ, the Peclet number, Pe, and the aspect ratio, α. If we assume two-dimensional flow, then substitution of Eq. 7 into Eqs. 1-3, 5 and 6 gives the following equations:

$$\frac{\partial v_x}{\partial x}+\frac{\partial v_z}{\partial z}=0 \tag{8}$$

$$\frac{\partial \Pi}{\partial x}=-v_x \tag{9}$$

$$\frac{\partial \Pi}{\partial z}=-v_z-\Lambda y \tag{10}$$

$$\frac{\partial y}{\partial \tau}+v_x\frac{\partial y}{\partial x}+v_z\frac{\partial y}{\partial z}=\frac{1}{Pe}\left(\frac{\partial^2 y}{\partial x^2}+\frac{\partial^2 y}{\partial z^2}\right)+1 \tag{11}$$

$$\begin{aligned} &y=0 \quad v_z=1 \quad \text{at} \quad z=0\\ &\frac{\partial y}{\partial z}=0 \quad \Pi=\Pi_0 \quad \text{at} \quad z=1\\ &v_x=0 \quad \frac{\partial y}{\partial x}=0 \quad \text{at} \quad x=0,\alpha \end{aligned} \tag{12}$$

In many packed beds, the Peclet number is large. In those cases we can simplify the model by neglecting the conduction of heat. For this simplified *convection-reaction model*, Eq. 11 becomes

$$\frac{\partial y}{\partial \tau}+v_x\frac{\partial y}{\partial x}+v_z\frac{\partial y}{\partial z}=1 \tag{13}$$

The simplified model has only two parameters, Λ and α, and can be solved much easier than the model with finite Peclet number.

To simplify the derivation of these equations, we ignored the viscosity variation with temperature. The same equations are obtained when this effect is included (in a linear approximation), but now the parameter Λ is defined by:

$$\Lambda=\frac{SL_1\kappa}{\mu_0 u_0^2 \rho_0 C_{pf}}\left(gb\rho_0-\frac{\mu_0 b^* u_0}{\kappa}\right)$$

where μ_o is the viscosity at the inlet and b^* is the coefficient in the approximation:

$$\mu=\mu_0[1-b^*(T-T_0)]$$

For liquids b^* is usually positive, whereas for gases it is negative.

Figure 1 shows the two-dimensional packed bed with the corresponding boundary conditions.

Linear Stability Analysis

For the trivial one-dimensional solution, we assume that there is no x or time dependency. We use the subscript b (= base case) for this solution. The continuity equation is then simply

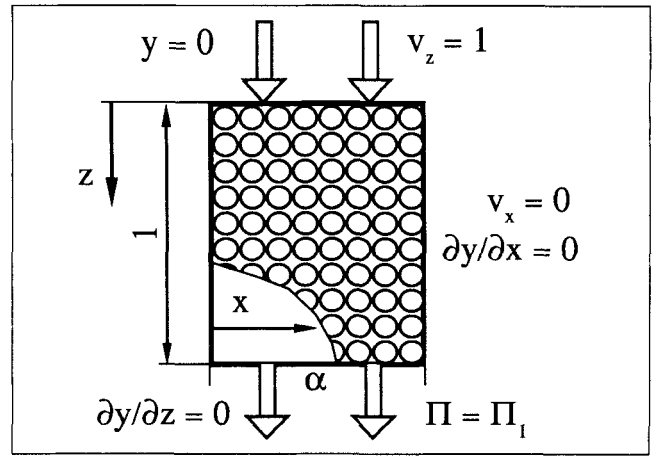

Figure 1. Packed bed with boundary conditions.

$$v_{xb}=0 \quad v_{zb}=1 \tag{14}$$

Integration of the energy balance gives

$$y_b=z+\frac{1}{Pe}\left[e^{-Pe}-e^{Pe(z-1)}\right] \tag{15}$$

Substitution of Eq. 15 into the momentum balance and integration with the boundary conditions gives:

$$\Pi_b=C-z-\Lambda\left[\frac{z^2}{2}+\frac{z}{Pe}e^{-Pe}-\frac{1}{Pe^2}e^{Pe(z-1)}\right] \tag{16}$$

where C is a constant of integration.

We examine now the stability of this solution. To reduce the number of equations in the two-dimensional system, we substitute the momentum balance, Eqs. 9 and 10, into the continuity equation and the energy balance, Eqs. 8 and 11

$$\frac{\partial^2 \Pi}{\partial x^2}+\frac{\partial^2 \Pi}{\partial z^2}+\Lambda\frac{\partial y}{\partial z}=0 \tag{17}$$

$$\frac{\partial y}{\partial \tau}=\frac{\partial \Pi}{\partial x}\frac{\partial y}{\partial x}+\frac{\partial \Pi}{\partial z}\frac{\partial y}{\partial z}+\frac{1}{Pe}\left(\frac{\partial^2 y}{\partial x^2}+\frac{\partial^2 y}{\partial z^2}\right)+\Lambda\frac{\partial y}{\partial z}y+1 \tag{18}$$

The corresponding boundary conditions are:

$$\begin{aligned} &y=0 \quad \frac{\partial \Pi}{\partial z}=-1 \quad \text{at} \quad z=0\\ &\frac{\partial y}{\partial z}=0 \quad \Pi=\Pi_0 \quad \text{at} \quad z=1\\ &\frac{\partial \Pi}{\partial x}=0 \quad \frac{\partial y}{\partial x}=0 \quad \text{at} \quad x=0,\alpha \end{aligned} \tag{19}$$

We transform the variables by subtracting the base-case solution

$$\begin{aligned} P&=\Pi-\Pi_b\\ Y&=y-y_b \end{aligned} \tag{20}$$

so that the trivial solution is always zero. Substitution of Eqs.

15-16 and 20 into Eqs. 17-19 gives

$$0=\frac{\partial^2 P}{\partial x^2}+\frac{\partial^2 P}{\partial z^2}+\Lambda\frac{\partial Y}{\partial z}$$

$$\frac{\partial Y}{\partial \tau}=\frac{\partial Y}{\partial x}\frac{\partial P}{\partial x}+\frac{\partial Y}{\partial z}\frac{\partial P}{\partial z}+\frac{1}{Pe}\left(\frac{\partial^2 Y}{\partial x^2}+\frac{\partial^2 Y}{\partial z^2}\right)$$

$$+\Lambda Y\frac{\partial Y}{\partial z}-\frac{\partial Y}{\partial z}+[1-e^{Pe(z-1)}]\left(\frac{\partial P}{\partial z}+\Lambda Y\right) \quad (21)$$

with the boundary conditions

$$\frac{\partial P}{\partial z}=0 \quad Y=0 \quad \text{at} \quad z=0$$

$$P=0 \quad \frac{\partial Y}{\partial z}=0 \quad \text{at} \quad z=1$$

$$\frac{\partial P}{\partial x}=0 \quad \frac{\partial Y}{\partial x}=0 \quad \text{at} \quad x=0,\alpha \quad (22)$$

Note that Eqs. 21-22 have a reflectional (Z_2) symmetry about the x axis: i.e., if $[P(x,z), Y(x,z)]$ is a solution, so is $[P(\alpha-x,z), Y(\alpha-x,z)]$. The Neumann boundary condition also introduces some hidden symmetries. Due to these symmetries, the nontrivial solutions always come in pairs (Crawford et al., 1991). The effect of symmetry on the local bifurcation and stability behavior of the system will be discussed further in the next section.

Equation 21 is of the form

$$C\frac{dX}{d\tau}=F(X,\Lambda) \quad (23)$$

where the capacitance matrix is

$$C=\begin{pmatrix}0 & 0\\ 0 & 1\end{pmatrix}$$

The nonlinear function F is the righthand side of Eq. 21, and the vector X is $(P, Y)^t$. The linearization of Eq. 23 around the trivial solution is:

$$C\frac{dw}{d\tau}=Lw \quad (24)$$

where the linear operator $L = D_xF(0, \Lambda)$ is defined by

$$Lw=\begin{pmatrix}\dfrac{\partial^2 w_1}{\partial x^2}+\dfrac{\partial^2 w_1}{\partial z^2}+\Lambda\dfrac{\partial w_2}{\partial z}\\ \dfrac{1}{Pe}\left(\dfrac{\partial^2 w_2}{\partial x^2}+\dfrac{\partial^2 w_2}{\partial z^2}\right)-\dfrac{\partial w_2}{\partial z}+[1-e^{Pe(z-1)}]\left(\dfrac{\partial w_1}{\partial z}+\Lambda w_2\right)\end{pmatrix} \quad (25)$$

with $w=(w_1, w_2)^t$. For the simplified convection-reaction model, the linear operator becomes

$$Lw=\begin{pmatrix}\dfrac{\partial^2 w_1}{\partial x^2}+\dfrac{\partial^2 w_1}{\partial z^2}+\Lambda\dfrac{\partial w_2}{\partial z}\\ -\dfrac{\partial w_2}{\partial z}+\dfrac{\partial w_1}{\partial z}+\Lambda\, w_2\end{pmatrix} \quad (26)$$

The corresponding boundary conditions are given by Eq. 22 with w_1 and w_2 standing for P and Y, respectively. Writing $w=ue^{\nu\tau}$ leads to the following eigenvalue problem for the linearized system

$$\nu Cu=Lu \quad (27)$$

To solve Eq. 27, we assume a solution of the form

$$u_1=f_{i1}(z)\cos\left(\frac{m\pi x}{\alpha}\right)$$

$$u_2=f_{i2}(z)\cos\left(\frac{m\pi x}{\alpha}\right) \quad (28)$$

Equation 28 satisfies the boundary conditions in x-direction. The index m specifies the mode number of the horizontal eigenfunction, and the index i the mode number of the vertical eigenfunction. Substitution of Eq. 28 into Eq. 27 gives

$$-\left(\frac{m\pi}{\alpha}\right)^2 f_{i1}+\frac{d^2 f_{i1}}{dz^2}+\Lambda\frac{df_{i2}}{dz}=0$$

$$\frac{1}{Pe}\left\{-\left(\frac{m\pi}{\alpha}\right)^2 f_{i2}+\frac{d^2 f_{i2}}{dz^2}\right\}-\frac{df_{i2}}{dz}+[1-e^{Pe(z-1)}]\left(\frac{df_1}{dz}+\Lambda f_{i2}\right)=\nu f_{i2}$$

with the boundary conditions

$$\frac{\partial f_{i1}}{\partial z}=0 \quad f_{i2}=0 \quad \text{at } z=0$$

$$f_{i1}=0 \quad \frac{\partial f_{i2}}{\partial z}=0 \quad \text{at } z=1 \quad (29)$$

To find the stationary stability boundary for the trivial solution we set $\nu=0$. (We could not find Hopf bifurcations where ν is purely imaginary). Then, for the simplified convection-reaction model, Eqs. 29 simplify to

$$\frac{d^3 f_{i1}}{dz^3}-\left(\frac{m\pi}{\alpha}\right)^2\frac{df_{i1}}{dz}+\Lambda\left(\frac{m\pi}{\alpha}\right)^2 f_{i1}=0$$

$$\frac{d^2 f_{i1}}{dz^2}+\left(\frac{m\pi}{\alpha}\right)^2 f_{i1}=0 \quad \frac{df_{i1}}{dz}=0 \quad \text{at } z=0$$

$$f_{i1}=0 \quad \text{at } z=1 \quad (30)$$

The linear stability boundary is given by the critical Λ for which the homogeneous system, Eqs. 29 or 30, has a nontrivial solution. We solved the system for the critical Darcy buoyancy number as a function of the aspect ratio using the shooting method. For each value of i and m, we get a different neutral

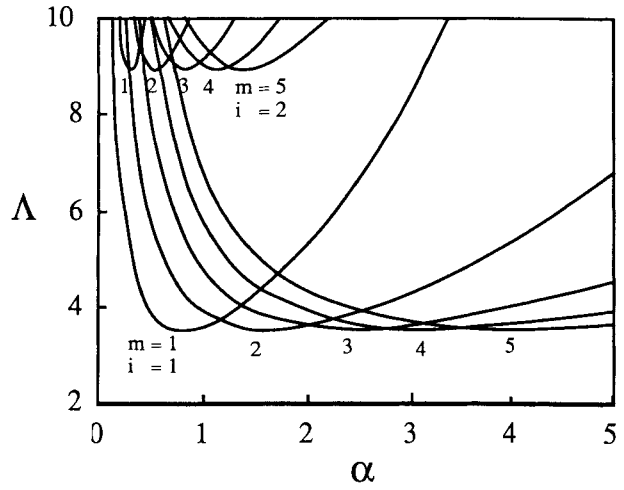

Figure 2. Neutral stability curves for simplified convection-reaction model.

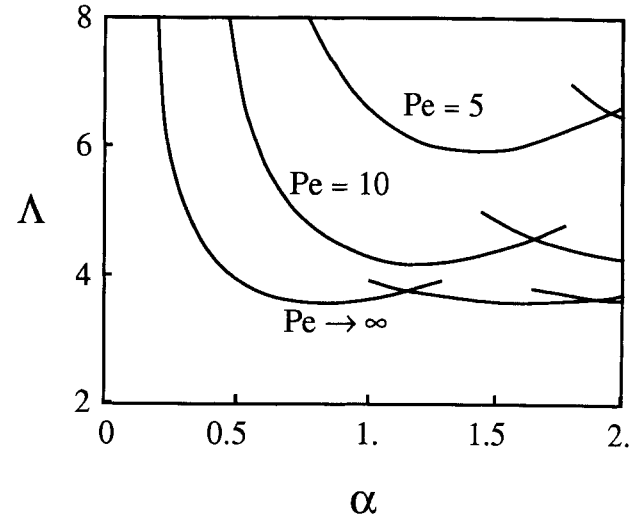

Figure 3. Neutral stability boundary for different Peclet numbers.

stability curve in the (Λ, α) space which indicates a zero eigenvalue. This is shown in Figure 2 for the simplified reaction-convection model. We see that all neutral stability curves, which come from large Λ values for small aspect ratios, have a minimum and go again to large Λ values for large aspect ratios. The minimum has the same value of Λ for all curves with the same mode number i (but different m). The mode number $i=1$ has the lowest critical Λ at 3.55. The curves with a mode number of $i=2$ have their minimum at $\Lambda \approx 9$. Higher mode numbers ($i>2$) lie above $\Lambda=10$ and are not shown in Figure 2. The trivial solution becomes unstable when the first eigenvalue crosses the imaginary axis. Thus, usually the modes with $i=1$ determine the stability of the system. If we speak in the following of a mode k solution, then this means that the vertical mode number $i=1$ and the horizontal mode number $m=k$.

For $\alpha<1.139$, the curve corresponding to mode 1 has the lowest value of Λ, for $1.139<\alpha<1.988$, the curve corresponding to mode 2 has the lowest value of Λ, and so on. For large aspect ratios, the critical Darcy buoyancy number remains nearly constant at the minimum value of $\Lambda_c=3.55$ because the minima become very flat and the curves lie closer together.

Figure 3 shows the neutral stability curves for different Peclet numbers. We see that increasing Peclet numbers shift the neutral stability curves downward and to the left until the curve of the simplified convection-reaction model is reached. This means that for a fixed aspect ratio, the uniform flow has a larger stability region and perturbations of lower mode numbers lead to the instability in the case of finite Peclet numbers than in the case of the simplified model. The curve for $Pe=20$ (not shown here) is only slightly different from the curve for $Pe\rightarrow\infty$. Because of the stiffness of the problem for large but finite Peclet numbers, we were not able to get any results for $Pe>20$.

By comparing these results with the neutral stability curves with Danckwerts boundary conditions we find that the flow with Danckwerts boundary conditions becomes unstable for slightly smaller Darcy buoyancy numbers. For example, for $Pe=5$, the minimum value of Λ is decreased by less than 10%; for $Pe=10$, it is decreased by less than 3%; and for $Pe=20$, the difference between the curves is less than 1%. For $Pe\rightarrow\infty$, both curves agree since the Hulburt and Danckwerts boundary conditions become identical for the simplified convection-reaction model.

No neutral stability curve exists for the negative values of Λ. This implies that viscosity variations with temperature alone (no density changes) cannot lead to flow maldistributions in the case of liquids.

Center Manifold Theory

To determine how the system behaves in the neighborhood of the limit of stability we perform a local analysis using the Center Manifold theorem. The theoretical background is described in much detail elsewhere (Holmes, 1981; Guckenheimer and Holmes, 1986; Wiggins, 1990). Therefore, we indicate only the key concepts and give the results. Because the analysis involves numerical calculations, we consider the local bifurcation behavior for the simplified convection-reaction model only. Similar calculations can be done for finite Peclet numbers.

To analyze the local bifurcation behavior of the original system, we expand the solution of Eq. 23 in terms of the eigenfunctions of the linearized system, Eq. 27.

$$X=\sum_{i=1}^{\infty} a_i \boldsymbol{u}_i \tag{31}$$

Substituting Eq. 31 into Eq. 23 and taking the inner product with the adjoint eigenfunctions transform the two partial differential equations into an infinite number of ordinary differential equations for the amplitudes a_i. The Center Manifold theorem implies that if a system of ordinary differential equations has k zero eigenvalues, then the local behavior in the neighborhood of this singular point is described by k ordinary differential equations. This means that for our case close to the limit of stability where one eigenvalue is zero, the local dynamic behavior of the system can be described by a single differential equation. If we use the index 1 for the eigenfunction with the zero eigenvalue, then this equation is of the form

Table 1. Coefficients in the Center Manifold reduction (Eq. 35)

$m\pi/\alpha$	A	B
3	1.17	1,140
4	1.30	1,490
5	1.36	4,530
6	1.40	36,200

$$\frac{da_1}{d\tau} = g_1(a_1,\lambda) \tag{32}$$

where

$$\lambda = \Lambda - \Lambda_c \tag{33}$$

The symmetry properties of the system can be used to show that the function $g_1(a_1,\lambda)$ must be of the form (Dangelmayr and Armbruster, 1986)

$$g_1(a_1,\lambda) = a_1 h_1(a_1^2,\lambda) = a_1[A\lambda + Ba_1^2 + Ca_1^4 + \ldots] \tag{34}$$

Equation 34 implies that the simplest possible bifurcation is a pitchfork. If $A,B \neq 0$, then the local bifurcation behavior is given by the truncated equation:

$$\frac{da_1}{d\tau} = a_1[A\lambda + Ba_1^2] \tag{35}$$

This equation is called the normal form of the bifurcation (the coefficients A and B are often scaled to unity). The calculation of coefficients A and B involves the solution of linear inhomogeneous partial differential equations and evaluation of some inner products. In the present case, it can be done only numerically and approximately as shown in the Appendix. In Table 1, the numerically calculated coefficients are presented for some values of $m\pi/\alpha$. (We see from Figure 2 that the smallest value of $m\pi/\alpha$ on the neutral stability curve is 2.8.) Coefficient A is always positive as expected, because the trivial solution is locally stable for Λ values below the neutral stability curve. Coefficient B is found to be positive, which means that the pitchfork is subcritical. A qualitative picture of a subcritical pitchfork bifurcation is given in Figure 4. We see that the local analysis using the normal form does not find a new stable state of the system after the uniform flow becomes unstable.

It is an unexpected result that the bifurcation in our problem is subcritical because most systems that have been analyzed in literature, namely the Benard problem and the Lapwood problem, exhibit supercritical bifurcations. In those cases, there is a smooth transition from the one-dimensional base case to two- or three-dimensional solutions. When the trivial solution becomes unstable in our problem, then there is a sudden change in the flow pattern. This corresponds to a first-order phase transition in thermodynamics.

At some critical values of the aspect ratio, two modes become unstable at the same time. The first three aspect ratios are $\alpha = 1.139$ with the modes $(m=1)$ and $(m=2)$, $\alpha = 1.988$ with the modes $(m=2)$ and $(m=3)$, and $\alpha = 2.814$ with the modes $(m=3)$ and $(m=4)$. At these singular points, two zero eigenvalues exist. The Center Manifold theorem implies that the

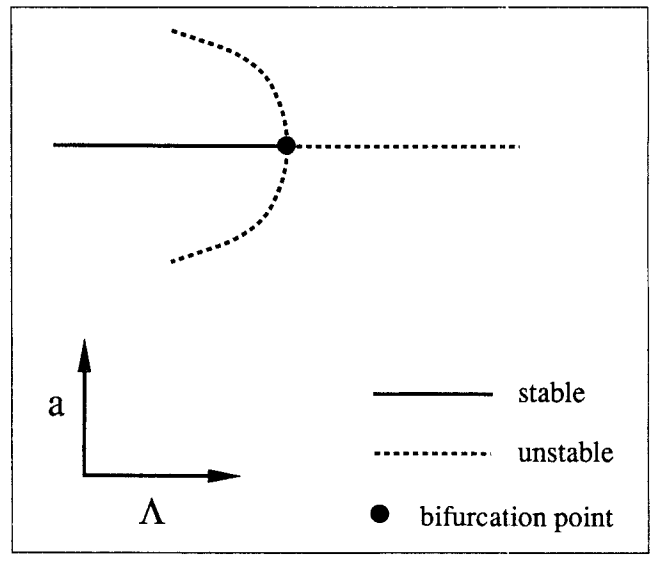

Figure 4. Subcritical pitchfork bifurcation.

local bifurcation picture in the neighborhood of those points is described by two ordinary differential equations.

$$\frac{da_1}{d\tau} = g_1(a_1,a_2,\lambda,\sigma)$$

$$\frac{da_2}{d\tau} = g_1(a_1,a_2,\lambda,\sigma) \tag{36}$$

where

$$\sigma = \alpha - \alpha_0 \tag{37}$$

is a new distinct parameter and α_o is the value of the aspect ratio at the double-zero eigenvalue. Dangelmayr and Armbruster (1986) show that for the systems with Neumann boundary conditions, the local dynamic behavior for the case of mode 1 and mode 2 interactions is given by the truncated equations

$$\frac{da_1}{d\tau} = A\lambda a_1 + B\sigma a_1 + Ca_1a_2$$

$$\frac{da_2}{d\tau} = D\lambda a_2 + E\sigma a_2 + Fa_1^2 + Ga_2^3 \tag{38}$$

For all other mode interactions, the local dynamic behavior is given by

$$\frac{da_1}{d\tau} = A\lambda a_1 + B\sigma a_1 + Ca_1^3 + Da_1a_2^2$$

$$\frac{da_2}{d\tau} = E\lambda a_2 + F\sigma a_2 + Ga_2a_1^2 + Ha_2^3 \tag{39}$$

The coefficients in Eq. 38, which correspond to the aspect ratio $\alpha = 1.139$, can be calculated similarly to the case of one-zero eigenvalue as shown in the Appendix and they are approximately

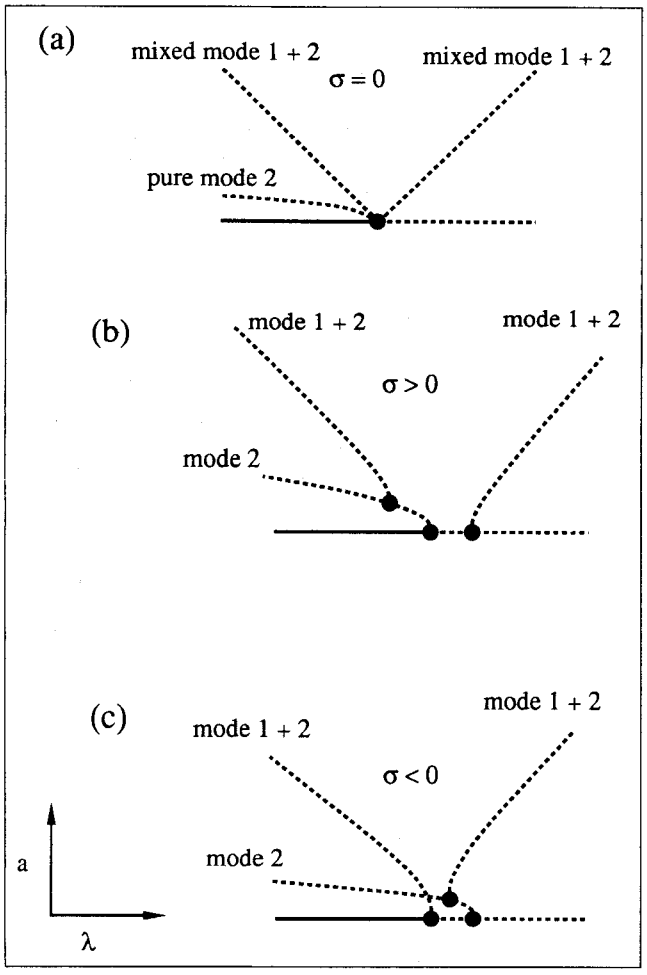

Figure 5. Local bifurcations in the neighborhood of double-zero eigenvalue at $\alpha = 1.139$.

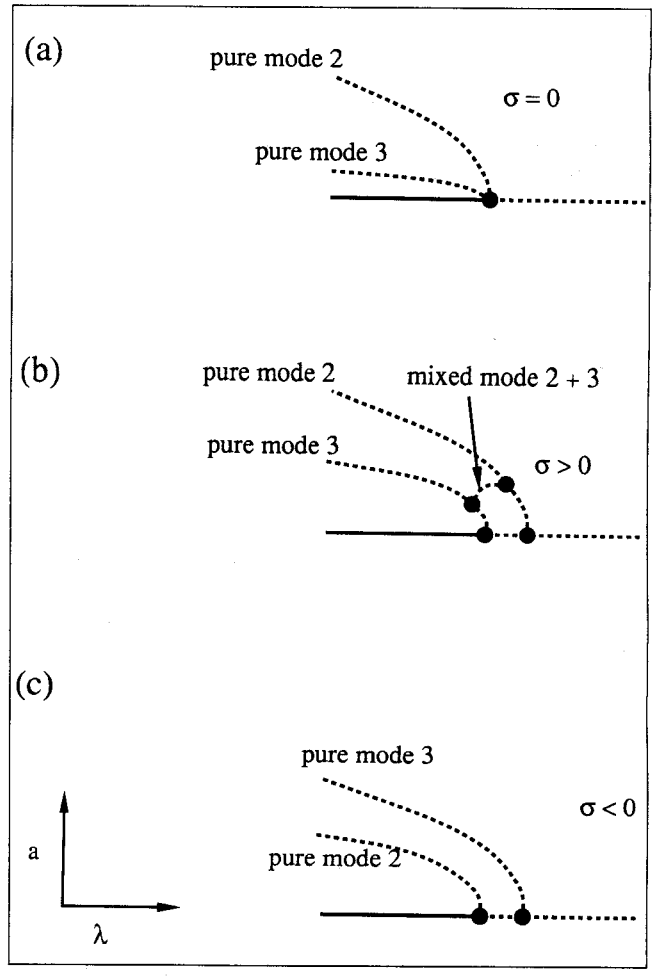

Figure 6. Local bifurcations in the neighborhood of double-zero eigenvalue at $\alpha = 1.988$.

$$A = 1.13 \quad B = -1.16 \quad C = 230 \quad D = 1.4$$
$$E = 1.27 \quad F = 0.81 \quad G = 8{,}500 \qquad (40)$$

The analysis of Eq. 38 with the coefficients in Eq. 40 is qualitatively different for $\sigma > 0$ and $\sigma < 0$. The qualitative unperturbed ($\sigma = 0$) bifurcation picture is given by Figure 5a. Two solutions (one mixed mode and one pure mode 2) bifurcate subcritically, and one mixed mode solution bifurcates supercritically from the trivial solution, but all are unstable. For $\sigma \neq 0$, there are two bifurcation points on the trivial branch. For $\sigma > 0$, the pure mode 2 solution bifurcates first subcritically. From the pure-mode branch, a mixed-mode solution bifurcates again subcritically. After the pure mode, the second mixed mode bifurcates from the trivial solution supercritically (see Figure 5b). For $\sigma < 0$, a mixed-mode solution bifurcates first from the trivial solution subcritically. Then, the pure mode bifurcates subcritically. From the pure-mode branch, the second mixed mode solution bifurcates supercritically. But all nontrivial solutions are unstable close to the bifurcation points (see Figure 5c).

For $\alpha = 1.988$ where the modes $m = 2$ and $m = 3$ become unstable at the same time, the coefficients of Eq. 39 can be calculated numerically to be approximately (see Appendix)

$$A = 1.20 \quad B = -0.039 \quad C = 950 \quad D = 21{,}000$$
$$E = 1.35 \quad F = 0.018 \quad G = -1{,}400 \quad H = 3{,}300 \qquad (41)$$

The bifurcation diagram of Eq. 39 with the coefficients given in Eq. 41 is shown in Figure 6a for $\sigma = 0$. Two pure modes, $m = 2$ and $m = 3$, bifurcate subcritically from the trivial solution at the same point. Both branches are unstable, and no mixed mode solution exists. For the case of $\sigma \neq 0$, the two solutions corresponding to modes 2 and 3 bifurcate subcritically at different points from the trivial solution. For $\sigma < 0$, no mixed mode exists. For $\sigma > 0$, a mixed mode connects the two pure-mode branches. Stability analysis of Eq. 37 on the mixed-mode solution shows that this branch is unstable. Figures 6b and 6c show the qualitative local picture for $\sigma < 0$ and $\sigma > 0$, respectively. Details on how to determine such local pictures can be found in Golubitsky and Schaeffer (1985).

The local bifurcation pictures of the solutions in the neighborhood of two-zero eigenvalues derived so far do not exhibit any stable branch other than the trivial one. This is due to the fact that most bifurcations are subcritical and that we included only terms up to order three in the Center Manifold reduction. To find stable solutions we need more terms in the amplitude equations (at least up to order five). Because it is difficult (and

only approximate) to determine these higher-order coefficients in the amplitude equations, we analyze the problem differently.

Numerical Solution by Orthogonal Collocation

We try to solve the problem given by Eqs. 21 and 22 using orthogonal collocation as described by Finlayson (1980). A simple way to do this is to approximate the solution as the sum of the first few eigenfunctions of the linearized system. This is possible in x-direction where the eigenfunctions are cosine functions. Unfortunately, the eigenfunctions in z-direction are not known explicitly and we have to approximate the solution by other orthogonal functions. The boundary conditions allow us to use trigonometric functions:

$$P(x,z,t)=\sum_{m=0}^{M}\sum_{n=0}^{N}a_{mn}(t)\cos\left(\frac{\pi m x}{\alpha}\right)\cos\left(\frac{(2n+1)\pi z}{2}\right)$$

$$Y(x,z,t)=\sum_{m=0}^{M}\sum_{n=0}^{N}b_{mn}(t)\cos\left(\frac{\pi m x}{\alpha}\right)\sin\left(\frac{(2n+1)\pi z}{2}\right) \qquad (42)$$

With the orthogonal collocation method we can reduce the two partial differential equations into $2(M+1)(N+1)$ algebraic-differential equations for the coefficients. They are of the form

$$\boldsymbol{M}\boldsymbol{a}=\boldsymbol{N}\boldsymbol{b} \qquad (43)$$

$$\boldsymbol{Q}\frac{d\boldsymbol{b}}{dt}=\boldsymbol{G}(\boldsymbol{a},\boldsymbol{b}) \qquad (44)$$

where the vectors $\boldsymbol{a}$ and $\boldsymbol{b}$ stand for all coefficients a_{mn} and b_{mn}, $\boldsymbol{M}$, $\boldsymbol{N}$ and $\boldsymbol{Q}$ are matrices, and $\boldsymbol{G}$ is a nonlinear function. Since the momentum balance, Eq. 43, is linear and $\boldsymbol{M}$ is invertible, the vector $\boldsymbol{a}$ can be expressed as a function of $\boldsymbol{b}$. In our special case, the relation between $\boldsymbol{a}$ and $\boldsymbol{b}$ is simply

$$a_{mn}(t)=b_{mn}(t)\,\frac{\Lambda\pi\,\dfrac{2n+1}{2}}{\left(\dfrac{\pi m}{\alpha}\right)^2+\left\{\dfrac{\pi(2n+1)}{2}\right\}^2} \qquad (45)$$

This simple relation is only possible if Hulburt boundary conditions are used. With Eq. 45 the problem can be reduced to one-vector equation

$$\boldsymbol{Q}\frac{d\boldsymbol{b}}{dt}=\boldsymbol{G}^*(\boldsymbol{b}) \qquad (46)$$

To find the steady states of the system we require the righthand side of Eq. 46 to be zero and solve for $\boldsymbol{b}$. This can be done with any nonlinear equation solver. Here, the Newton method is used. To find the stability of the solutions we linearize the operator $\boldsymbol{Q}^{-1}\boldsymbol{G}^*$ around the steady state and determine the eigenvalues. If all eigenvalues have negative real parts, then the solution is stable. At points where two eigenvalues cross the imaginary axis, Hopf bifurcation occurs. Thus, we can find the starting points for oscillating solutions as well, if they occur.

The numerical effort is proportional to $[(M+1)(N+1)]^2$, because we need the Jacobian matrix of the system for the Newton method and the stability calculations. The accuracy of the collocation method depends on the chosen values of N and M. Because we used the eigenfunctions in x-direction as approximating functions, we expect them to be very accurate. The main error is due to poor approximation of the profiles in z-direction. Our calculations showed that the eigenvalues (which determine the stability) are more sensitive with respect to the order of approximation than the solution curve itself. The error can be estimated by comparing solutions with different values of M and N. Using these error estimates we expect our results (calculated with $M=4$ and $N=15$) to be very accurate close to the uniform flow, but far away from the base case the error may be as large as 5%. We found also that M must be at least twice the mode number of a solution branch to get correct results. Therefore, we restrict our analysis to mode numbers of two or less.

The advantage of the numerical method compared with the Center Manifold method is that we get a picture that is valid globally. The local analysis is also limited by the increasing difficulties to determine the higher-order coefficients. The disadvantage of the collocation method is that we do not know how many solutions exist or in which direction they bifurcate. The approximation can also give rise to spurious solutions, if the values of M and N are not chosen properly. Thus, the best way to find the bifurcation picture is to use the knowledge of the Center Manifold reduction as the starting point for the collocation method. Then, we know how many solutions bifurcate from the trivial solution where the bifurcation points are and in which direction they go. The branches can be followed by using a continuation scheme (Kubicek and Marek, 1983).

Another advantage of the collocation method is that we get without additional calculations the flow patterns and temperature distributions. One has to substitute only the computed coefficients into Eq. 42 and to add the base-case solution.

Due to the large number of collocation points that results in a large number of ODE's, we were not able to follow the time-dependent solution branches. To identify these solutions, we integrated Eq. 46 with a few arbitrarily chosen initial conditions. In most cases, this method led to one of the stable steady-state solution branches. However, we were able to find stable time-dependent solutions in parameter regions where no stable steady-state solutions exist.

Description of Maldistributed Flows and Isotherms

In Figure 7 we show qualitatively the streamlines and temperature distributions for all steady-state solutions that occur in our bifurcation diagrams. The cases without stagnation points are shown first. The one-dimensional flow is shown in Figure 7a. Here, the streamlines are parallel and the temperature increases uniformly. In Figure 7b the solution that corresponds to the eigenfunction of mode one is shown. We see that there is a region of slow flow at one side. The fluid in this region has a longer residence time and, therefore, a higher temperature due to the constant heat source. There exists also a solution that is the mirror image of this solution because of

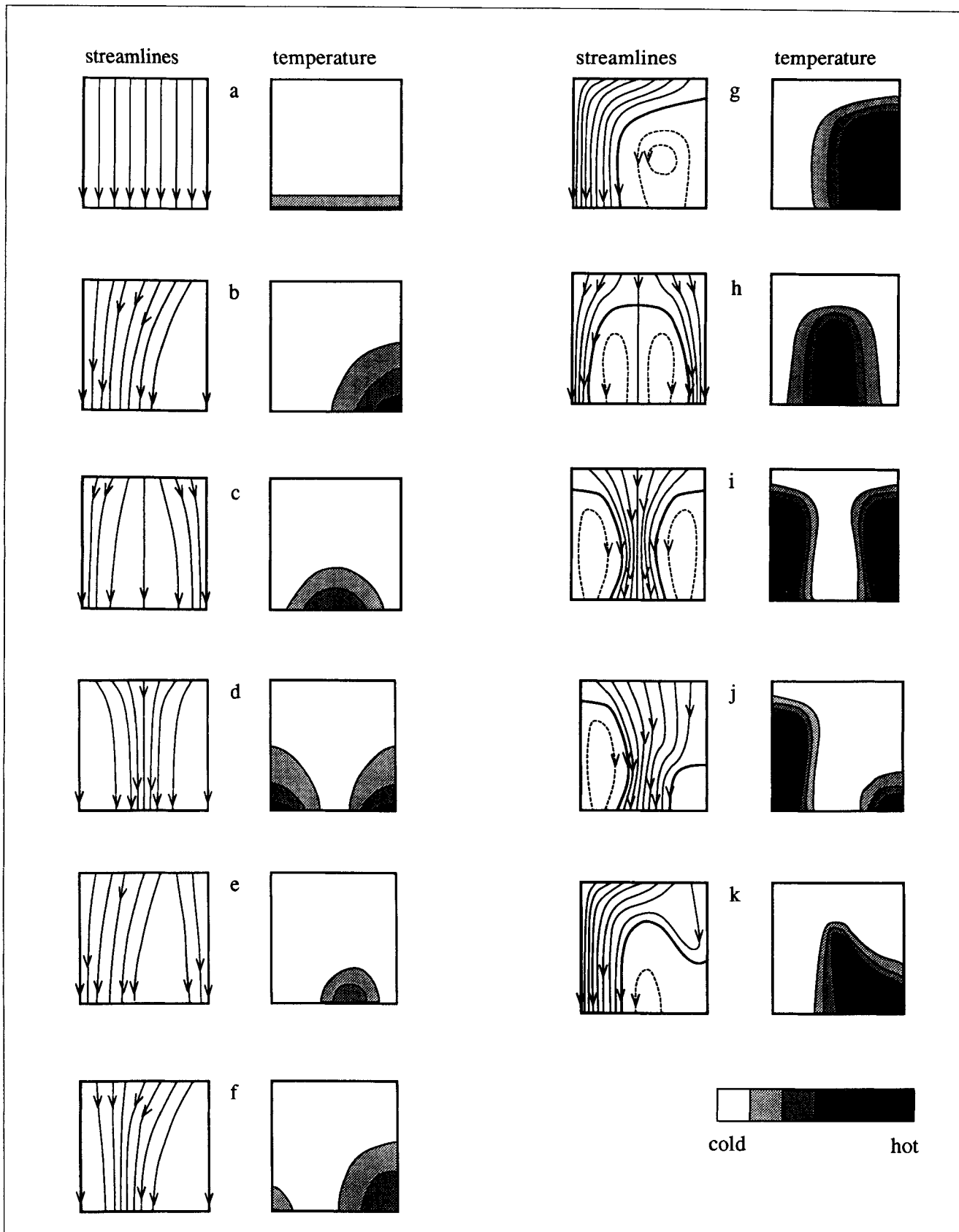

Figure 7. Streamlines and temperature distribution for all steady-state solutions (mode 1 + 2).

the symmetry properties of the problem. The streamlines and temperature distribution corresponding to a mode-two eigenfunction are shown in Figures 7c and 7d. Here, the slow flow is either in the reactor middle or close to the walls, which gives rise to one hot spot at the bottom middle or to two hot spots in the lower corners of the reactor. In Figures 7e and 7f we see the solution corresponding to a 1-2 mixed-mode eigenfunction. In the first case, most of the flow is at one side, but there is also flow at the other wall. The slow flow region is on one side but not at the wall, and the corresponding hot spot is at the bottom. In the other case, the fast flow is at one side but not at the wall. This gives rise to a hot spot in one corner and to a smaller hot spot in the other corner. Both mixed-mode solutions have also a mirror image due to symmetry.

If one or more stagnation points occur, then there exist one or more regions in the reactor that are separated from the through flow. Those zones are usually at the bottom of the reactor, but they can extend over large parts of the packed bed. We find in these regions flow from the bottom into the separated region, which leaves again at the bottom. Closed streamlines inside the separated zones are also possible. Because the fluid remains very long in these zones (the leaving fluid gets sucked up immediately), the temperature there is very high. The fluid that enters the reactor at the top must flow around the stagnant regions and has a much shorter residence time than in the case of uniform flow. The temperature increase, however, is about the same due to the conduction of heat from the hot stagnant region.

In Figure 7g we show the streamlines and temperature distribution corresponding to a mode-one eigenfunction. The stagnant region is in the lower right corner, which gives rise to a hot spot there. The streamlines in the stagnant region are indicated by broken lines. Again, there exists a mirror image of this solution as well. Figures 7h and 7i show the streamlines and temperature distributions corresponding to a mode-two eigenfunction. There either is a stagnant region at the bottom middle or are two stagnant regions in the lower corners. Due to the long residence time, the temperature is high in these regions. In Figures 7j and 7k we see the streamlines and temperature distributions corresponding to a mixture of mode-one and mode-two eigenfunctions. Either there is one stagnant region in the center which extends to one corner or there are two stagnant regions in the lower corners but of different size. Again, these zones are the sites of the hot spots.

There are also time-dependent solutions. These are not necessarily periodic, but they all follow the same scheme which is shown in Figures 8a and 8b. The streamlines of the time-dependent solutions are shown qualitatively in Figure 8a. First, the flow is very similar to the uniform flow, but then a slow flow region forms in one lower corner. The flow becomes slower until a stagnation point occurs in the lower corner and moves upward. This gives rise to a stagnant region, which becomes larger and larger. Because the stagnant region extends

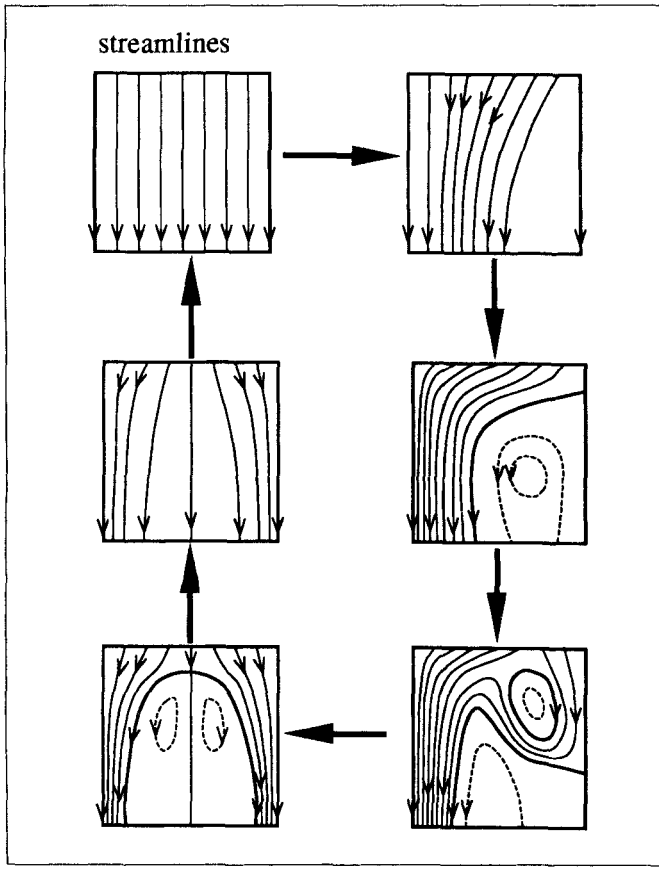

Figure 8a. Streamlines for time-dependent solutions.

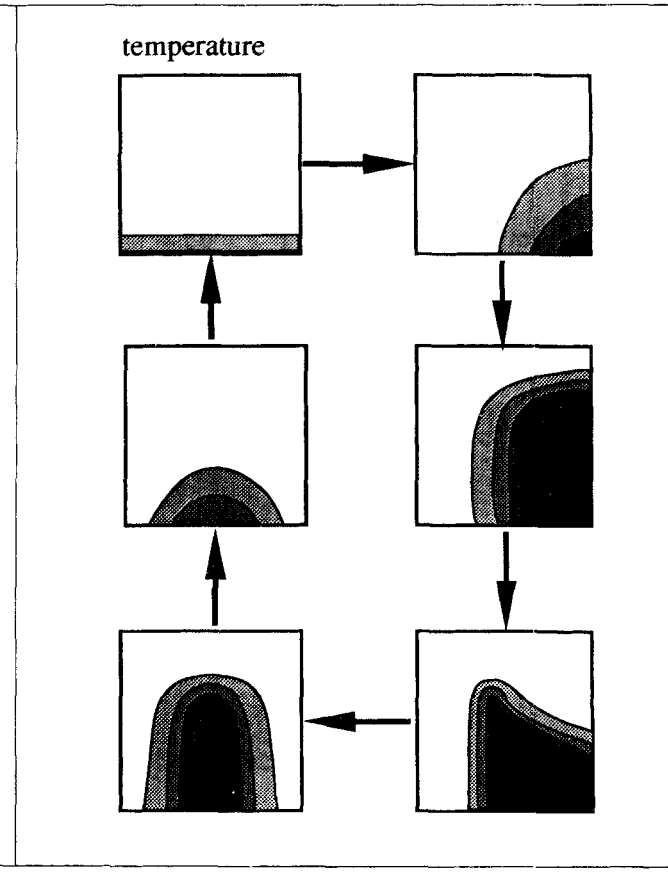

Figure 8b. Temperature distribution for time-dependent solutions.

further into the middle of the reactor, the stagnation point at the wall (which is now nearly at the top of the reactor) moves downward. This causes another separated region in the upper corner that is surrounded by the through flow. When the stagnation point reaches the lower corner, through flow on this side is possible, forcing the two stagnant regions to move closer together. This causes the two separated regions to unify and to form one stagnant region in the bottom middle of the reactor. First, this stagnant region is large but then the stagnation point moves from close to the top to the bottom. Thus, the stagnant region ceases to exist, and only a slow flow region in the reactor middle is left. This slow flow also vanishes and the streamlines are parallel again. Now, a new slow flow region forms either in the same corner as before or in the other corner and the cycle starts again.

The corresponding temperature profiles are shown in Figure 8b. Starting from the one-dimensional temperature profile, a hot spot forms in one corner. It becomes bigger, and its highest point moves from the wall into the middle of the reactor. Then, the whole hot region leaves the wall and moves into the middle. There, the temperature and size of the hot spot decreases until the base case is reached again. Then, a new hot spot forms in the same corner or in the other corner and so on.

Bifurcation Diagrams

We now present numerically computed bifurcation diagrams for several sets of Pe and α values. As it is not possible to quantitatively show the bifurcation diagrams of systems that have three or more degrees of freedom, we only provide a qualitative description as a projection in the two-dimensional space. The stable branches are solid lines, the unstable branches are broken lines, and the time-dependent solutions (which we found) are little dots. The large dots indicate a bifurcation point or a limit point and are marked with the corresponding value of Λ. The numerical calculations show that the identification of nontrivial solutions by the mode numbers, as derived in the local analysis, is valid only in a very small neighborhood of the bifurcation point. If we move along a nontrivial solution branch, other modes soon contribute to the solution and can become as important as the original mode. We identify a branch always with the mode number of the unstable eigenfunction at its origin.

The letters indicate which type of streamlines and temperature distributions exist along the branches. Because of the reflectional symmetry, all branches come in pairs. For solutions containing odd-mode eigenfunctions (in our examples mode-1 and mixed-mode solutions), the stability of both branches is identical and we show only one of them. Pairs of branches corresponding to even modes, however, have usually different stabilities and different secondary bifurcation points. Thus, we plot both curves in these cases. Due to numerical limitations, we could not follow all branches very far and, therefore, some of the diagrams are incomplete.

Figure 9 shows the bifurcation diagram for $Pe = 5$ and $\alpha = 2$. The behavior close to the trivial solution is in agreement with the local analysis for $Pe \to \infty$ in the neighborhood of a double-zero eigenvalue. The uniform flow becomes unstable at $\Lambda = 6.5$, where two mode-2 solutions bifurcate subcritically, implying that they are unstable close to the bifurcation point. Both branches reach a limit point at $\Lambda = 4.2$, but only the upper one (which corresponds to a hot spot in the middle) becomes stable. The lower branch has a secondary bifurcation point at $\Lambda = 6.4$, where a mixed-mode solution branches off. This mixed-mode solution reaches a limit point at $\Lambda = 4.2$ and becomes stable. Shortly after the limit point, however, a Hopf bifurcation occurs and the solution is unstable again. The mixed-mode branch reaches another limit point at $\Lambda = 6.8$ before it comes back to the trivial solution from where it bifurcates supercritically. It never becomes stable after the Hopf bifurcation point. The lower mode-2 solution branch has another secondary bifurcation after the limit point at $\Lambda = 4.4$, but it does not become stable nor is the new mixed-mode solution branch stable. We were not able to find any stable time-dependent solutions for these parameter values. We see also from the bifurcation diagram that flow without stagnant regions exists only in the neighborhood of the trivial solution. This implies that only solutions with stagnant regions are stable (here the solution with flow patterns of type h and g).

Figure 10 shows the bifurcation diagram for $Pe = 5$ and $\alpha = 1.5$. Here, the uniform flow becomes unstable at $\Lambda = 5.9$

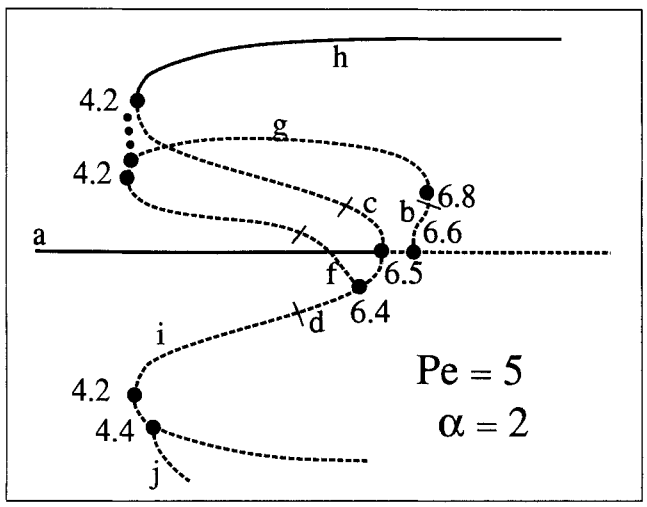

Figure 9. Bifurcation diagram for $Pe = 5$ and $\alpha = 2.0$.

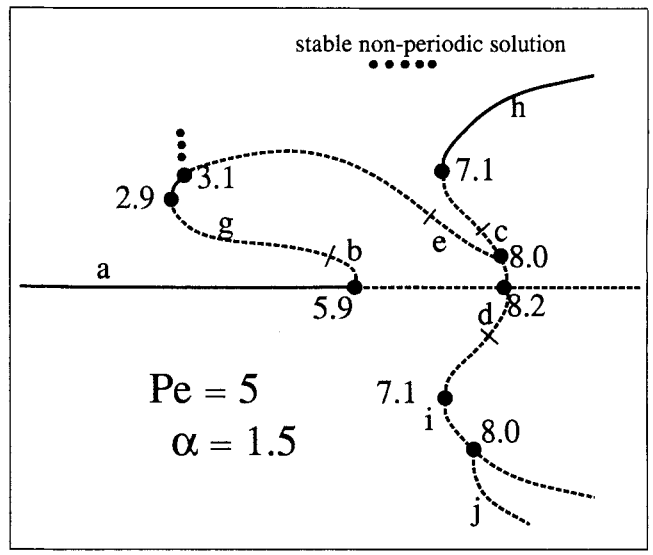

Figure 10. Bifurcation diagram for $Pe = 5$ and $\alpha = 1.5$.

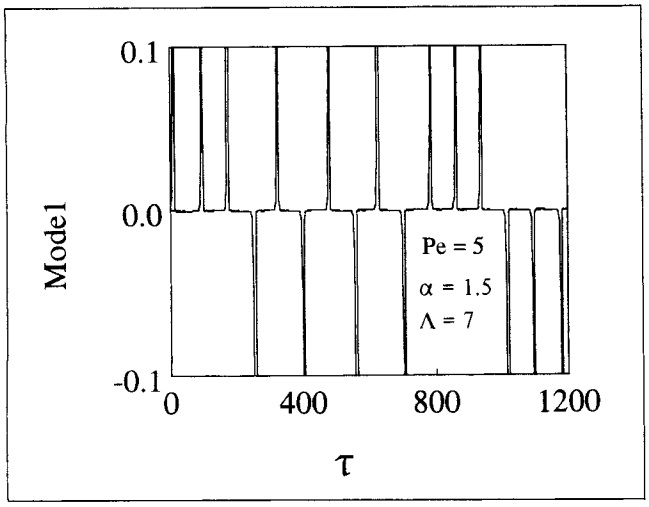

Figure 11. Leading coefficient of mode-one eigenfunction as a function of time for the time-dependent solution in Figure 10.

where a mode-1 solution bifurcates subcritically. This branch reaches a limit point at $\Lambda = 2.9$ and becomes stable. At $\Lambda = 3.1$, a Hopf bifurcation occurs and the solution becomes unstable again. The branch ends at $\Lambda = 8$, where it bifurcates from the upper mode-2 solution branch. The two mode-2 branches bifurcate subcritically from the uniform solution at $\Lambda = 8.2$. Both reach a limit point at $\Lambda = 7.1$ and the upper branch becomes stable. The lower branch has also a secondary bifurcation at $\Lambda = 8$, but after the limit point. This branch and the new mixed-mode solution remain unstable. We could not find stable time-dependent solutions close to the Hopf bifurcation point. However, in the region between $\Lambda = 5.9$ and 7.1 where no steady-state solutions exist, a nonperiodic (chaotic) solution as described in Figures 8a and 8b was found. This solution remained mostly at the uniform flow, and the flow maldistributions occurred only for a short period of time. Figure 11 shows how the leading coefficient of mode 1 changes with time for $\Lambda = 7$. It is not possible to predict on which side the hot spot occurs. The time between the occurrence of the hot spots is also not constant but varies between $\tau = 68$ and 84. Because of this behavior, we suspect that the system is in the neighborhood of a homoclinic orbit. However, this conjecture remains to be verified. Figure 10 shows that a direct transition from the uniform flow to the time-dependent, nonperiodic flow is possible.

Figure 12 shows the bifurcation diagram for $Pe = 5$ and $\alpha = 1$. We see that the uniform flow becomes unstable at $\Lambda = 6.5$ where a mode 1 solution bifurcates subcritically. It reaches a limit point at $\Lambda = 4.2$ and becomes stable. At $\Lambda = 4.3$, the solution turns back again and becomes unstable. Another limit point is reached at $\Lambda = 4.1$, but the solution remains unstable until a Hopf bifurcation point is reached at $\Lambda = 13.3$. The stable branch ends at $\Lambda = 13.4$ where it bifurcates from the upper mode-2 solution branch. Mode-2 solutions bifurcate subcritically from the trivial solution at $\Lambda = 13.4$. Both reach a limit point at $\Lambda = 13.2$ but do not become stable. The upper branch, however, becomes stable at $\Lambda = 13.4$, where the mixed-mode solution bifurcates. Again, we were able to find stable, time-dependent solutions as described in Figures 8a and 8b in the region without stable steady-state solutions. These solutions were found to be periodic. Either the hot spot remained always on one side or the location of the hot spot was alternating. As in all bifurcation diagrams that we showed so far, only solutions with stagnant regions are stable (here solutions of type g, h and k). The dimensionless temperature (which corresponds to the temperature rise) in the hot spots of the stable solutions with stagnant regions is two to five times higher than the highest temperature of the uniform flow.

Figure 13 show the bifurcation diagram for $Pe = 5$ and $\alpha = 0.5$. Here, the uniform flow becomes unstable at $\Lambda = 13.4$ where a mode-1 solution bifurcates subcritically. The branch reaches a limit point and becomes stable at $\Lambda = 13.2$. At $\Lambda = 40.7$, the branch reaches another limit point and becomes unstable. At $\Lambda = 28$, a Hopf bifurcation occurs; and at $\Lambda = 25.5$, the branch turns back again, but it does not become stable. At $\Lambda = 31.6$ another mode-1 (but mode 2 in vertical direction) solution bifurcates subcritically from the uniform solution. It reaches a limit point at $\Lambda = 29.2$, but remains unstable. At $\Lambda = 40$, the mode-two solutions branch supercritically from the uniform flow, but are unstable. For this small aspect ratio, none of the solutions have a stagnant region. This has the effect that the dimensionless temperature (which corresponds to the temperature rise) in the hot spots is only about 20%

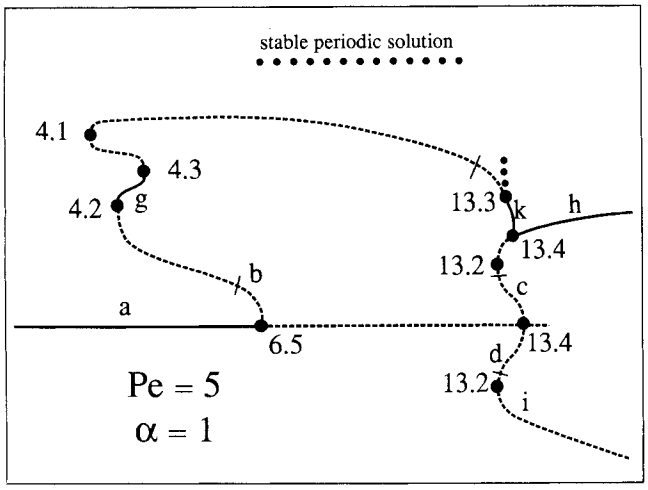

Figure 12. Bifurcation diagram for $Pe = 5$ and $\alpha = 1.0$.

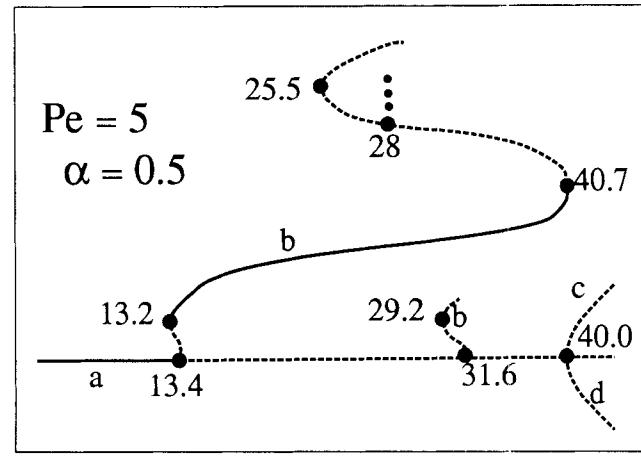

Figure 13. Bifurcation diagram for $Pe = 5$ and $\alpha = 0.5$.

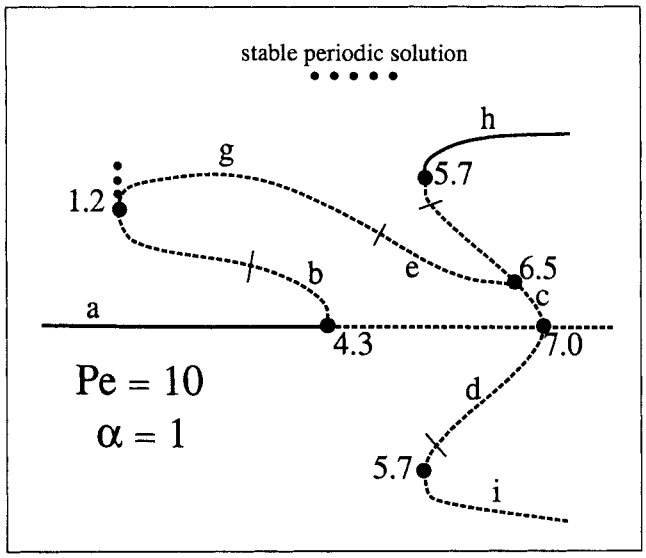

Figure 14. Bifurcation diagram for $Pe = 10$ and $\alpha = 1.0$.

higher than the temperature at the bottom of the uniform flow.

Figure 14 shows the bifurcation diagram for $Pe = 10$ and $\alpha = 1$. Here, the uniform flow becomes unstable at $\Lambda = 4.3$, where a mixed-mode solution bifurcates subcritically. At $\Lambda = 1.2$, this branch has a limit point and becomes stable. However, immediately after the limit point, a Hopf bifurcation occurs and the branch becomes unstable. It remains unstable until it ends at $\Lambda = 6.5$ where it bifurcates from the upper mode-two solutions branch. The mode-two solutions bifurcate from the uniform flow at $\Lambda = 7$. Both reach a limit point at $\Lambda = 5.7$, but only the upper one becomes stable. Again, we find a stable periodic solution as described in Figures 8a and 8b between $\Lambda = 4.3$ and $\Lambda = 5.7$, where no stable steady-state solution exists. All stable solutions have stagnant regions and dimensionless temperature in the hot spots for $Pe = 10$ is about twice as high as for $Pe = 5$.

Figure 15 shows the bifurcation diagram for $Pe = 2.5$ and $\alpha = 1$. It looks qualitatively very similar to the one for $Pe = 5$ and $\alpha = 1$. The only difference is that the mode-2 solutions branch off supercritically from the trivial solution for $Pe = 2.5$ (at $\Lambda = 33$). The uniform flow becomes unstable at $\Lambda = 14.4$, where mode-1 solution branches off subcritically. It reaches a limit point at $\Lambda = 13$ and becomes stable until $\Lambda = 16.5$ where the branch turns back. Another limit point is reached at $\Lambda = 15$, but the solution remains unstable. At $\Lambda = 38.7$ a Hopf bifurcation occurs and the branch becomes stable until it meets the upper mode-2 solution branch at $\Lambda = 39.5$. This mode-2 solution branch becomes stable after the mixed-mode solution bifurcates. The other mode-2 solution branch is not stable. We were also able to find a stable periodic solution in the region where no stable steady-state solution exists. We see also that solutions without stagnation point exist only in the neighborhood of the trivial solution branch. All stable solutions exhibit stagnant regions.

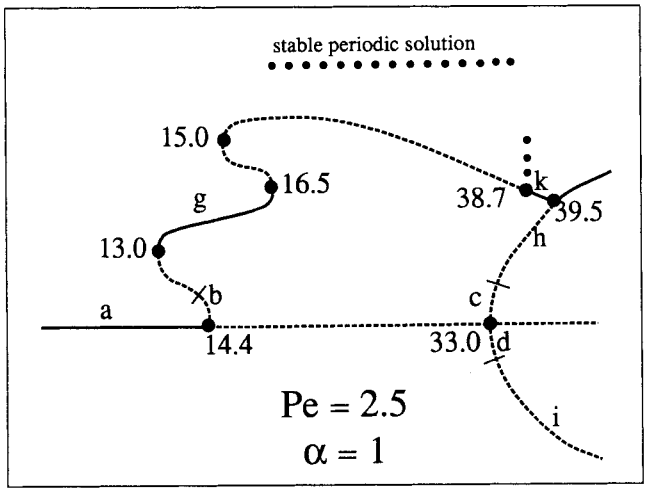

Figure 15. Bifurcation diagram for $Pe = 2.5$ and $\alpha = 1.0$.

Structural Stability of the Simplified Convection-Reaction Model

In this section we consider the global solution diagram of the simplified convection-reaction model. We can solve this model similar to the model with finite Peclet number using orthogonal collocation. Figures 16 and 17 show the numerically computed bifurcation diagrams for the two values of the aspect ratio, $\alpha = 1.0$ and 1.4. The local bifurcation diagrams are in qualitative agreement with the center manifold predictions shown in Figure 5. However, the global solution diagrams do not contain a stable branch for the values of Λ exceeding Λ_c, the value of the linear stability limit. The bifurcation diagrams in Figures 16 and 17 show only modes 1 and 2 to be unstable. However, all higher modes not shown were also found to be unstable. When the numerical algorithm was forced to find (stable) solutions for $\Lambda > \Lambda_c$, spurious solutions were obtained, which moved away to infinity as the number of terms in the approximation was increased. From these observations, we conclude that the simplified convection-reaction model is structurally unstable: i.e., the global solution diagrams of Eq. 21 for any large, but finite, Peclet number are different from those of the simplified convection-reaction model.

We note that the simplified convection-reaction model cannot predict a stagnation point. If there is a point with zero

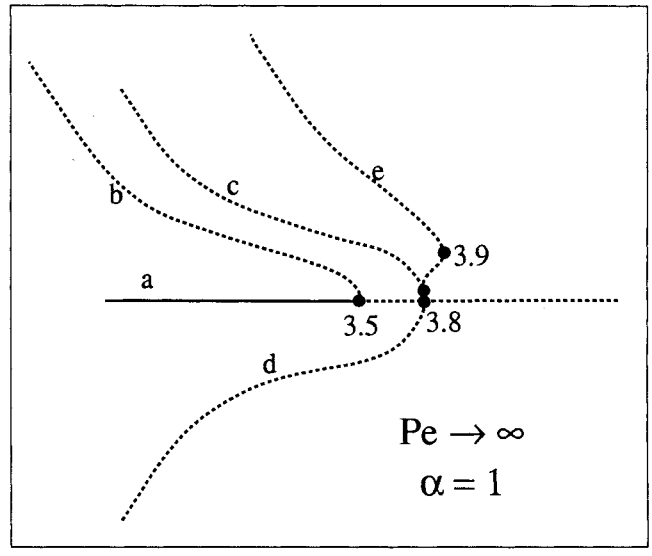

Figure 16. Bifurcation diagram of simplified convection-reaction model for $\alpha = 1.0$.

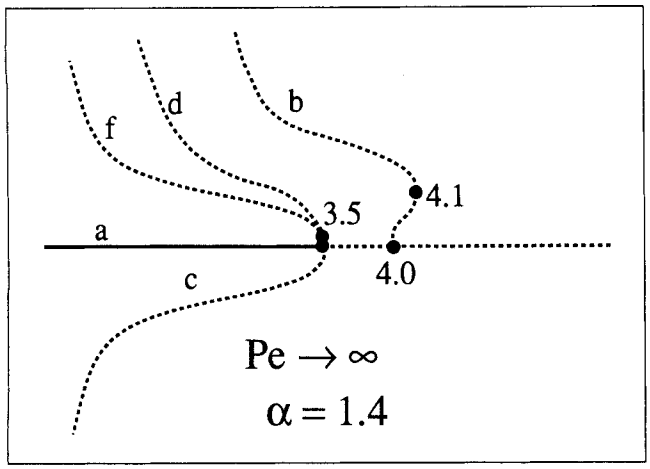

Figure 17. Bifurcation diagram of simplified convection-reaction model for $\alpha = 1.4$.

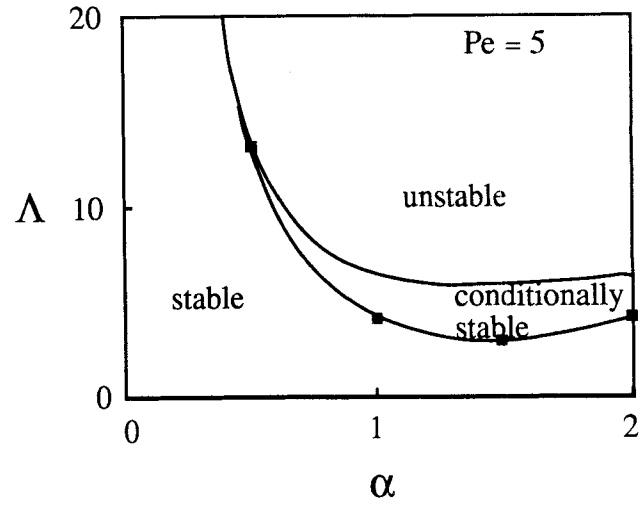

Figure 18. Stability boundaries of uniform flow for $Pe = 5$.

velocity, then with a constant heat source the temperature at that point will go to infinity without heat removal by conduction. Thus, the simplified convection-reaction model excludes a whole class of solutions containing a stagnation point.

The structural stability of the simplified model is probably due to the fact that the convection is the only mechanism to remove the heat generated by the constant heat source. Since the heat removal is not proportional to the local temperature and even more a high temperature decreases the heat removal, the system may not be able to exhibit stable, nonuniform solutions. If another mechanism to remove heat is added or if the heat generation is limited by considering reactant consumption, then we expect the convection-reaction model to be structurally stable. It is also possible that the Boussinesq approximation leads to the structural instability of the model. If this approximation is replaced by a physically meaningful one over the entire temperature range, then it may be possible for the simplified convection-reaction model to have stable, nonuniform solutions.

Conclusions and Discussion

We derived a simple two-dimensional model and used it to simulate flow maldistributions in homogeneous packed-bed reactors with down flow. Using linear stability analysis, we found the critical Darcy buoyancy number as a function of the aspect ratio. When the parameters are above this boundary, the uniform flow becomes unstable. Local bifurcation techniques were used to show that at the limit of stability a subcritical pitchfork bifurcation occurs. With the local theory as a guide, we used the orthogonal collocation and continuation techniques to follow the solution branches and compute the bifurcation diagrams for several aspect ratios and Peclet numbers. The streamlines and temperature profiles for the branches were also determined. The two-dimensional solutions exhibit regions with low and high flow rates, and correspondingly hot and cold spots. The results show that the transitions from one solution to another are not smooth. When the uniform flow becomes unstable, e.g., by decreasing the flow rate, there is a sudden change to a two-dimensional solution which is stable. Even a direct transition from uniform flow to periodic or chaotic behavior is possible.

An interesting result is that there is a wide region, in which the uniform flow is stable but other two-dimensional solutions are stable as well. The one-dimensional flow is unconditionally stable (i.e., stable to all disturbances) for Λ values below at the left most limit point of the bifurcation diagrams. Using these numerically computed values, we can construct an additional stability boundary in the (α,Λ) and (Pe,Λ) planes. This is shown in Figures 18 and 19. We see the neutral stability curves from the linear stability analysis and below them the curves corresponding to the limit points from the bifurcation diagrams. (The calculated values are marked.) For parameter values below the lower line, the uniform flow is stable. For parameter values between the two lines, the uniform flow is stable to small disturbances but may become unstable to finite disturbances. Above the upper curve (linear stability boundary), the uniform flow is unstable. We see from the diagrams that the region where the uniform flow is only conditionally stable increases with increasing Pe. For increasing values of α, the conditionally stable region increases first until the Λ values of both curves remain more or less constant. For small

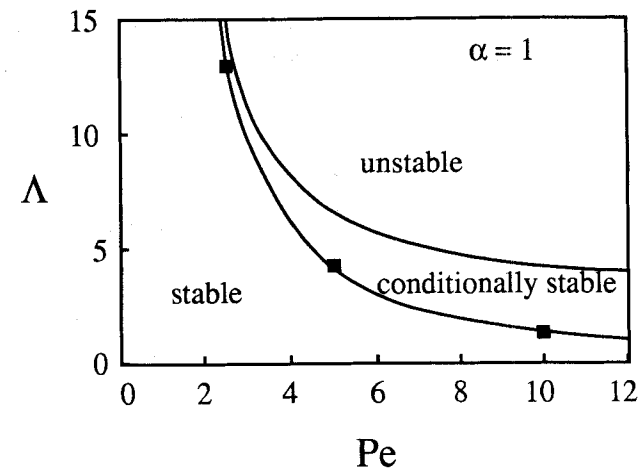

Figure 19. Stability boundaries of uniform flow for $\alpha = 1.0$.

Table 2. Typical Parameter Values for Packed Beds

Liquid	Gas
$\rho_{of} = 800$ .. (1,500) .. 2,000 kg/m^3	$\rho_{of} = 0.1$. (1) .. 10 kg/m^3
$C_{pf} = 1{,}000$ .. (1,500) .. 4,000 J/kg·K	$C_{pf} = 500$. (1,000) .. 2,000 J/kg·K
$u_o = 0.001$ .. (0.01) .. 0.1 m/s	$u_o = 0.01$ .. (0.07) .. 0.3 m/s
$\lambda_{eff} = 1$ .. (2) .. 7 W/m·K	$\lambda_{eff} = 0.3$ .. (0.8) .. 2 W/m·K
$b = 0.0002$. (0.001) . 0.002 L/K	$b = 0.002$. (0.003) . 0.004 L/K
$T_o = 300$ .. (500) .. 600 K	$T_o = 300$ .. (650) .. 900 K
$\mu_o = 0.0001$ .. (0.001) .. 0.1 kg/m·s	$\mu_o = 10^{-5}$. $(3 \cdot 10^{-5})$. 10^{-4} kg/m·s

$D_p = 0.002$ .. (0.01) . 0.02 m
$L_1 = 0.1$ .. (1) .. 10 m
$\epsilon = 0.3$ .. (0.4) .. 0.6
$g = 9.81$ m/s^2
$\kappa = 10^{-9}$ .. (10^{-7}) .. 10^{-6} m^2

values of α and Pe, the two stability boundaries are nearly identical. These phase diagrams, Figures 18 and 19, are useful for predicting *a priori* the parameter values, for which flow maldistributions can exist.

We could determine the lower stability boundary in Figures 18 and 19 only after extensive numerical calculations. Sometimes it is possible to obtain a conservative approximation to this boundary using the energy stability method (Serrin, 1959; Joseph, 1965, 1966). We have not been successful in deriving such a boundary as the present problem does not admit a variational formulation. Homsy and Sherwood (1976) derived the linear and energy stability limits for convective instability in a through-flow system with fixed-temperature boundary conditions. In the case of large Peclet numbers (for which all the temperature rise is at the exit of the bed), these authors obtain the critical Darcy buoyancy numbers to be 14.3 (linear stability limit) and 5.77 (energy limit). Because of the large difference between the two values, Homsy and Sherwood (1976) conjectured that there may be subcritical bifurcation in their problem. However, no calculations were done to verify the conjecture.

After obtaining the critical values of Λ for flow maldistributions, we examine if these values are within the possible range for packed beds. The Darcy buoyancy number may be written as:

$$\Lambda = \left(\frac{Ra}{Pe}\right)\beta \tag{47}$$

where

$$\beta = \frac{\Delta T}{T_0} \qquad \frac{Ra}{Pe} = \frac{\rho_0 g \kappa b T_0}{u_0 \mu_0} \tag{48}$$

β is the dimensionless temperature rise of the uniform flow, Ra is the Rayleigh number, and Pe is the Peclet number.

In Table 2 we see typical values of the dimensional quantities for liquids and gases as given in Salisbury (1962), Perry and Green (1984), and Vortmeyer et al. (1974). The table shows a possible range of values as well as one typical example. The definition of the permeability κ is given by Eq. 4. Substitution of those values into Eq. 48 shows a large range of possible values.

$$\left(\frac{Ra}{Pe}\right)_{\text{liquid}} = 5 \cdot 10^{-5} \text{ .. } (75) \text{ .. } 2 \cdot 10^{5}$$

$$\left(\frac{Ra}{Pe}\right)_{\text{gas}} = 2 \cdot 10^{-4} \text{ .. } (0.6) \text{ .. } 4 \cdot 10^{3}$$

The geometric mean of the maximum and minimum, which is usually a good guess for a typical value, is $Ra/Pe \approx 3$ for both gases and liquids. A typical β value is about 0.1 to 0.3 so that the Darcy buoyancy number has the same order of magnitude as the critical value derived in our analysis. Therefore, the one-dimensional flow can become unstable in real packed beds.

The Darcy buoyancy number depends mostly on the packing of the bed and the viscosity. For very fine packing and high viscous fluids, we get small values of Λ for large particles, and low viscous fluids we get very high values of Λ. Thus, a way to avoid instabilities is to use smaller catalyst pellets or larger flow rates. However, higher velocities will lead to shorter residence times and hence low conversion.

The analysis here was restricted to a single fluid and a two-dimensional packed bed, although most real packed (or trickle)-bed reactors are three-dimensional and involve more than one fluid. However, we expect that the same mechanisms lead to the instability of the uniform flow.

Acknowledgment

This work is supported by grants from the Texas Advanced Research Program, American Chemical Society Petroleum Research Fund and the Robert A. Welch Foundation.

Notation

a = coefficient of amplitude equation
b = coefficient of thermal expansion
b^* = coefficient for viscosity change with temperature
b = coefficient of amplitude equation
C_p = heat capacity
D = width of the packed bed
D_p = mean particle diameter
e = unit vector
F = nonlinear operator
g = acceleration due to gravity
i = vertical mode number
L = vertical direction
L = linearized operator
m = horizontal mode number
p = pressure

P = transformed dimensionless pressure
Pe = Peclet number
Ra = Rayleigh number
s = horizontal direction
S = source term
t = time
T = temperature
u = velocity or eigenfunction
v = dimensionless velocity or adjoint eigenfunction
w = variables of linearized problem
x = dimensionless horizonal direction
X = vector of variables
y = dimensionless temperature
Y = transformed dimensionless temperature
z = dimensionless vertical direction

Greek letters

α = aspect ratio, D/L
β = dimensionless source term
ϵ = void fraction of packed bed
κ = permeability
λ_{eff} = effective thermal diffusivity
λ = $(\Lambda - \Lambda_c)$
Λ = Darcy buoyancy number
μ = viscosity
ν = eigenvalue
Π = dimensionless pressure
ρ = density
σ = $(\alpha - \alpha_o)$
τ = dimensionless time

Subscripts

b = base case
c = critical
i = corresponding to mode number i
L = vertical direction
o = reference value at inlet
s = horizontal direction
x = horizontal direction
z = vertical direction
1 = at exit

Literature Cited

Bdzil, J. B., and H. L. Frisch, "Chemically Driven Convection," *J. Chem. Phys.*, **72**, 1875 (1980).

Bird, R. B., W. E. Stewart, and E. N. Lightfoot, *Transport Phenomena*, Wiley, New York (1960).

Chow, S. N., and J. K. Hale, *Methods of Bifurcation Theory*, Springer-Verlag, New York (1982).

Crawford, J. D., M. Golubitsky, M. G. M. Gomes, E. Knobloch, and I. N. Stewart, "Boundary Conditions As Symmetry Constraints," *Singularities, Bifurcations and Dynamics*, Workshop Proc., Springer-Verlag, Heidelberg in press (1991).

Dangelmayr, G., and D. Armbruster, "Steady State Mode Interaction in the Presence of O(2) Symmetry and in Nonflux Boundary Conditions," *Cont. Math.*, **56**, 53 (1986).

Finlayson, B. A., *Nonlinear Analysis in Chemical Engineering*, McGraw-Hill, New York (1980).

Gasser, R. D., and M. S. Kazimi, "Onset of Convection in a Porous Medium with Internal Heat Generation," *ASME Trans. J. Heat Transfer*, **98**, 49 (1976).

Gatica, J. E., H. J. Viljoen, and V. Hlavacek, "Influence of Secondary Flows on the Stability of Chemically Reacting Systems," *AIChE J.*, **34**, 209 (1988).

Gatica, J. E., H. J. Viljoen, and V. Hlavacek, "Interaction between Chemical Reaction and Natural Convection in Porous Media," *Chem. Eng. Sci.*, **44**, 1853 (1989).

Gershuni, G. Z., and E. M. Zhukhivutskii, *Convective Stability of Incompressible Fluids* (Transl. from Russian), Keter Publishing House, Jerusalem (1976).

Golubitsky, M., and D. G. Schaeffer, *Singularities and Groups in Bifurcation Theory*, Vol. 1, Springer, New York (1985).

Guckenheimer, J., and P. Holmes, *Nonlinear Oscillations, Dynamical Systems, and Bifurcations of Vector Fields*, Springer-Verlag, New York (1986).

Hadim, A., and L. C. Burmeister, "Onset of Convection in a Porous Medium with Internal Heat Generation and Downward Flow," *J. Thermophysics*, **2**, 343 (1988).

Holmes, P. J., "Center Manifolds, Normal Forms and Bifurcations of Vector Fields with Application to Coupling between Periodic and Steady Motions," *Physica 2D*, 449 (1981).

Homsy, G. M., and A. E. Sherwood, "Convective Instabilities in Porous Media with Through Flow," *AIChE J.*, **22**, 168 (1976).

Hulburt, H. M., "Chemical Processes in Continuous Flow Systems: Reaction Kinetics," *Ind. Eng. Chem.*, **36**, 1012 (1944).

Jaffe, S. B., "Hot Spot Simulation in Commercial Hydrogenation Processes," *Ind. Eng. Chem. Process Des. Dev.*, **15**, 411 (1976).

Jones, M. C., and J. M. Persichetti, "Convective Instability in Packed Beds with Through Flow," *AIChE J.*, **32**, 1555 (1986).

Joseph, D. D., "On the Stability of the Boussinesq Equations," *Arch. Rat. Mech. Anal.*, **20**, 59 (1965).

Joseph, D. D., "Nonlinear Stability of the Boussinesq Equations by the Method of Energy," *Arch. Rat. Mech. Anal.*, **22**, 163 (1966).

Kordylewski, W., and Z. Krajewski, "Convection Effects on Thermal Ignition in Porous Media," *Chem. Eng. Sci.*, **39**, 610 (1984).

Kubicek, M., and M. Marek, *Computational Methods in Bifurcation Theory and Dissipative Structures*, Springer, New York (1983).

Nield, D. A., "The Onset of Transient Convective Instability," *J. Fluid Mech.*, **71**, 441 (1975).

Nield, D. A., "Convective Instability in Porous Media with Through Flow," *AIChE J.*, **33**, 1222 (1987).

Perry, R. H., and D. W. Green, eds., *Perry's Chemical Engineers' Handbook*, 6th ed., McGraw-Hill, New York (1984).

Prasad, V., "Thermal Convection in a Rectangular Cavity Filled with a Heat-Generating, Darcy Porous Medium," *J. Heat Transfer*, **109**, 697 (1987).

Reda, D. C., "Mixed Convection in a Liquid-Saturated Porous Medium," *J. Heat Transfer*, **110**, 147 (1988).

Salisbury, J. K., ed., *Kent's Mechanical Engineers' Handbook*, 12th ed., Wiley, New York (1962).

Serrin, J., "On the Stability of Viscous Fluid Motions," *Arch. Rat. Mech. Anal.*, **3**, 1 (1959).

Steinberg, V., and H. Brand, "Convective Instabilities of Binary Mixtures with Fast Chemical Reaction in a Porous Medium," *J. Chem. Phys.*, **78**, 2655 (1983).

Stewart, Jr., W. E., and C. L. G. Dona, "Free Convection in a Heat-Generating Porous Medium in a Finite Vertical Cylinder," *J. Heat Transfer*, **110**, 517 (1988).

Stroh, F., "Reaction Induced Flow Maldistributions in Packed-Beds," PhD Thesis, Univ. of Houston, Houston (1991).

Sutton, F. M., "Onset of Convection in a Porous Channel with Net Through Flow," *Phys. Fluids*, **13**, 1931 (1970).

Tveitereid, M., "Thermal Convection in a Horizontal Porous Layer with Internal Heat Sources," *Int. J. Heat Mass Transfer*, **20**, 1045 (1977).

Viljoen, H. J., and V. Hlavacek, "Chemically Driven Convection in a Porous Medium," *AIChE J.*, **33**, 1344 (1987).

Vortmeyer, D., K. J. Dietrich, and K. O. Ring, "Comparison of One- and Two-Phase Model Predictions for Adiabatic Packed-Bed Chemical Reactors," *Adv. Chem. Ser.*, **133**, 588 (1974).

Wiggins, S., *Introduction to Applied Nonlinear Dynamical Systems and Chaos*, Springer-Verlag, New York (1990).

Wooding, R. A., "Rayleigh Instability of a Thermal Boundary Layer in Flow Through a Porous Medium," *J. Fluid Mech.*, **9**, 183 (1960).

Appendix: Derivation of Amplitude Equations for Simple- and Double-Zero Eigenvalue

After substitution of Eq. 32 into Eq. 23 and taking the inner product with the adjoint eigenfunction v_m, we get the amplitude equations:

$$\frac{da_m}{dt} = a_m\mu_m + \lambda \sum_{i=1}^{\infty} a_i \langle D^2_{x\lambda}F(\mathbf{0},0)u_i, v_m\rangle + \frac{1}{2!}\sum_{i=1}^{\infty}\sum_{j=1}^{\infty} a_i a_j \langle D^2_{xx}F(\mathbf{0},0)(u_i,u_j), v_m\rangle + \frac{1}{3!}\sum_{i=1}^{\infty}\sum_{j=1}^{\infty}\sum_{k=1}^{\infty} a_i a_j a_k \langle D^3_{xxx}F(\mathbf{0},0)(u_i,u_j,u_k), v_m\rangle + \ldots \quad m = 1, 2, \ldots, \infty \quad \text{(A1)}$$

where μ_m is the eigenvalue corresponding to the eigenfunction u_m, λ is defined in Eq. 33, $\langle , \rangle$ stands for the inner product, v_m is the normalized adjoint eigenfunction, and $D^2_{x\Lambda}F(\mathbf{0}, \Lambda_c)$, $D^2_{xx}F(\mathbf{0}, \Lambda_c)$, $D^3_{xxx}F(\mathbf{0}, \Lambda_c)$ are Frechet derivatives of the operator F (Chow and Hale, 1982). We assume that one eigenvalue is zero and all other eigenvalues have a negative real part.

$$\mu_1 = 0 \text{ and } Re(\mu_m) < 0 \quad m = 2, 3, \ldots, \infty \quad \text{(A2)}$$

The Center Manifold theorem then implies that the local dynamic behavior of system (Eq. A1) is described by a single ordinary differential equation, Eq. 33, and close to the zero eigenvalue, all amplitudes a_m can be expressed as:

$$a_m = h_m(a_1, \lambda) \quad m = 2, 3, \ldots, \infty \quad \text{(A3)}$$

where h_m contains only quadratic or higher-order terms in a_1 and λ. Therefore, we can write

$$a_m = \alpha_{m1}a_1^2 + \alpha_{m2}a_1\lambda + \alpha_{m3}\lambda^2 + \text{cubic terms} \quad m = 2, 3, \ldots, \infty \quad \text{(A4)}$$

We substitute Eq. A4 into Eq. A1 and solve for the α_{mi}. This gives

$$a_m = -\frac{\lambda a_1}{\mu_m}\langle D^2_{x\lambda}F(\mathbf{0},0)u_1, v_m\rangle - \frac{a_1^2}{2\mu_m}\langle D^2_{xx}F(\mathbf{0},0)(u_1, u_1), v_m\rangle + \text{cubic terms} \quad m = 2, 3, \ldots, \infty \quad \text{(A5)}$$

Substitution of Eq. A5 into Eq. A1 with $m = 1$ gives:

$$\frac{da_1}{dt} = \lambda a_1\langle D^2_{x\lambda}F(\mathbf{0},0)u_1, v_1\rangle + \frac{a_1^2}{2}\langle D^2_{xx}F(\mathbf{0},0)(u_1, u_1), v_1\rangle + \frac{a_1^3}{3!}\langle D^3_{xxx}F(\mathbf{0},0)(u_1, u_1, u_1), v_1\rangle - \frac{a_1^3}{2}\sum_{m=2}^{\infty}\frac{1}{\mu_m}\langle D^2_{xx}F(\mathbf{0},0)(u_1, u_1), v_m\rangle \cdot \langle D^2_{xx}F(\mathbf{0},0)(u_m, u_1), v_1\rangle + \text{terms of higher order} \quad \text{(A6)}$$

The quadratic (and all higher even order) terms vanish because of the symmetry of the problem. Equation 35 follows immediately from Eq. A6. In the case of two-zero eigenvalues, the local bifurcation behavior is determined by two amplitude equations which can be derived similarly. Using the symmetry properties, the normal forms can be determined (Dangelmayr and Armbruster, 1986). At a double-zero eigenvalue of mode $m = 1$ and $m = 2$, the local bifurcation behavior is given by:

$$\frac{da_1}{dt} = \lambda a_1\langle D^2_{x\lambda}F(\mathbf{0},\Lambda_c,\alpha_0)u_1, v_1\rangle + \sigma a_1\langle D^2_{x\alpha}F(\mathbf{0},\Lambda_c,\alpha_0)u_1, v_1\rangle + a_1a_2\langle D^2_{xx}F(\mathbf{0},\Lambda_c,\alpha_0)(u_1,u_2), v_1\rangle$$

$$\frac{da_2}{dt} = \lambda a_2\langle D^2_{x\lambda}F(\mathbf{0},\Lambda_c,\alpha_0)(u_2), v_2\rangle + \sigma a_2\langle D^2_{x\alpha}F(\mathbf{0},\Lambda_c,\alpha_0)(u_2), v_2\rangle + \frac{a_1^2}{2}\langle D^2_{xx}F(\mathbf{0},\Lambda_c,\alpha_0)(u_1,u_1), v_2\rangle - \sum_{m=3}^{\infty}\frac{a_2^3}{2\mu_m}\langle D^2_{xx}F(\mathbf{0},\Lambda_c,\alpha_0)(u_2,u_2), v_m\rangle \cdot \langle D^2_{xx}F(\mathbf{0},\Lambda_c,\alpha_0)(u_2,u_m), v_2\rangle \quad \text{(A7)}$$

and in the case of all other double-zero eigenvalues, the normal form is:

$$\frac{da_1}{dt} = \lambda a_1\langle D^2_{x\lambda}F(\mathbf{0},\Lambda_c,\alpha_0)(u_1), v_1\rangle + \sigma a_1\langle D^2_{x\alpha}F(\mathbf{0},\Lambda_c,\alpha_0)(u_1), v_1\rangle - \sum_{m=3}^{r}\frac{a_1^3}{2\mu_m}\langle D^2_{xx}F(\mathbf{0},\Lambda_c,\alpha_0)(u_1,u_1), v_m\rangle \cdot \langle D^2_{xx}F(\mathbf{0},\Lambda_c,\alpha_0)(u_1,u_m), v_1\rangle - \sum_{m=3}^{r}\frac{a_1a_2^2}{\mu_m}\langle D^2_{xx}F(\mathbf{0},\Lambda_c,\alpha_0)(u_1,u_2), v_m\rangle \cdot \langle D^2_{xx}F(\mathbf{0},\Lambda_c,\alpha_0)(u_2,u_m), v_1\rangle$$

$$\frac{da_2}{dt} = \lambda a_2\langle D^2_{x\lambda}F(\mathbf{0},\Lambda_c,\alpha_0)(u_2), v_2\rangle + \sigma a_2\langle D^2_{x\alpha}F(\mathbf{0},\Lambda_c,\alpha_0)(u_2), v_2\rangle - \sum_{m=3}^{r}\frac{a_2^3}{2\mu_m}\langle D^2_{xx}F(\mathbf{0},\Lambda_c,\alpha_0)(u_2,u_2), v_m\rangle \cdot \langle D^2_{xx}F(\mathbf{0},\Lambda_c,\alpha_0)(u_2,u_m), v_2\rangle - \sum_{m=3}^{r}\frac{a_2a_1^2}{\mu_m}\langle D^2_{xx}F(\mathbf{0},\Lambda_c,\alpha_0)(u_1,u_2), v_m\rangle \cdot \langle D^2_{xx}F(\mathbf{0},\Lambda_c,\alpha_0)(u_1,u_m), v_2\rangle \quad \text{(A8)}$$

Dangelmayr and Armbruster (1986) give the form of Eqs. A7 and A8, but not the expressions for the coefficients. A derivation of these coefficients is given by Stroh (1991). Equations 37 and 38 follow directly from Eqs. A7 and A8.

The Frechet derivatives for the simplified convection-reaction model are:

$$D^2_{x\Lambda}F(\mathbf{0},\ \Lambda_c)\boldsymbol{u}_1=\begin{pmatrix}\dfrac{\partial u_2}{\partial z}\\ u_2\end{pmatrix} \tag{A9}$$

$$D^2_{xx}F(\mathbf{0},\Lambda_c)(\boldsymbol{u}_1,\boldsymbol{w}_1)$$

$$=\begin{pmatrix}0\\ \dfrac{\partial u_2}{\partial x}\dfrac{\partial w_1}{\partial x}+\dfrac{\partial u_1}{\partial x}\dfrac{\partial w_2}{\partial x}+\dfrac{\partial u_2}{\partial z}\dfrac{\partial w_1}{\partial z}\\ +\dfrac{\partial u_1}{\partial z}\dfrac{\partial w_2}{\partial z}+\Lambda_c\left(u_2\dfrac{\partial w_2}{\partial z}+w_2\dfrac{\partial u_2}{\partial z}\right)\end{pmatrix} \tag{A10}$$

$$D^3_{xxx}F(\mathbf{0},\Lambda_c)(\boldsymbol{u}_1,\boldsymbol{u}_1,\boldsymbol{u}_1)=0 \tag{A11}$$

$$D^2_{x\alpha}F(\mathbf{0},\Lambda_c,\alpha_0)(\boldsymbol{u})=\begin{pmatrix}-\dfrac{2}{\alpha}\dfrac{\partial^2 u_1}{\partial x^2}\\ 0\end{pmatrix} \tag{A12}$$

The adjoint eigenvalue problem is:

$$\boldsymbol{v}\boldsymbol{C}\boldsymbol{v}=\boldsymbol{L}^*\boldsymbol{v}=\begin{pmatrix}\dfrac{\partial^2 v_1}{\partial x^2}+\dfrac{\partial^2 v_1}{\partial z^2}-\dfrac{\partial v_2}{\partial z}\\ \dfrac{\partial v_2}{\partial z}-\Lambda\dfrac{\partial v_1}{\partial z}+\Lambda\ v_2\end{pmatrix}$$

$$v_1=0 \quad v_2=0 \quad \text{at} \quad z=1$$

$$\frac{\partial v_1}{\partial z}-v_2=0 \quad \text{at} \quad z=0$$

$$\frac{\partial v_1}{\partial x}=\frac{\partial v_2}{\partial x}=0 \quad \text{at} \quad x=0,\alpha \tag{A13}$$

The adjoint eigenfunction $\boldsymbol{v}$ can be calculated numerically in the same way as the eigenfunction $\boldsymbol{u}$. The normalization condition is:

$$\langle \boldsymbol{C}\boldsymbol{u}_i,\boldsymbol{v}_i\rangle=1$$

The calculation of some of the coefficients involved infinite sums. Each term of the sum corresponds to one eigenfunction of the linearized system. If the corresponding eigenvalue is close to the origin, then this term is important. All terms that correspond to eigenvalues, which are far away from the origin, can be neglected. Thus, we used for the sum only those terms that correspond to the smallest eigenvalues (which have a magnitude of order 10 or less).

Manuscript received Oct. 2, 1990, and revision received Mar. 22, 1991.